

# Adhesion and electronic structure of graphene on hexagonal boron nitride substrates: First-principles investigation within the random phase approximation

B. Sachs,<sup>1,\*</sup> T. O. Wehling,<sup>1,†</sup> M. I. Katsnelson,<sup>2</sup> and A. I. Lichtenstein<sup>1</sup>

<sup>1</sup>*I. Institut für Theoretische Physik, Universität Hamburg, Jungiusstraße 9, D-20355 Hamburg, Germany*

<sup>2</sup>*Radboud University of Nijmegen, Institute for Molecules and Materials,*

*Heijendaalseweg 135, 6525 AJ Nijmegen, The Netherlands*

(Dated: January 28, 2019)

We investigate the adsorption of graphene sheets on h-BN substrates by means of first-principles calculations in the framework of adiabatic connection fluctuation-dissipation theory in the random phase approximation. We obtain adhesion energies for different crystallographic stacking configurations and show that the interlayer bonding is due to long-range van der Waals forces. The interplay of elastic and adhesion energies is shown to lead to stacking disorder. Band structure calculations reveal substrate induced mass terms in graphene which change their sign with the stacking configuration. Our results are in agreement with recent STM experiments.

PACS numbers: 81.05.ue; 73.22.Pr; 71.10.-w; 71.20.-b

The development of graphene-based nanoelectronic devices, such as high-speed transistors, calls for high electron mobilities. Currently, substrates beneath the graphene present an important source of disorder including corrugation effects of the graphene [1–3], charge traps [1, 4] and dangling bonds [5]. A promising candidate to become a new standard substrate material is hexagonal boron nitride (h-BN). This BN polymorph is remarkably similar to graphite: The alternating B and N atoms form two-dimensional layers of strong  $sp^2$  bonds within a honeycomb arrangement and a lattice constant which differs by less than 2% from that of graphene. The h-BN sheets are weakly bound by long-range adhesive forces at an equilibrium distance of  $3.3\text{\AA}$  [6]. The electronic structure, however, exhibits clear differences: the chemically inequivalent sublattices make h-BN an insulator with a band gap of 6.0 eV [7]. Recently, the fabrication of graphene devices on h-BN with highly improved electron mobilities and carrier inhomogeneities, reaching a quality comparable to suspended graphene has been reported [8, 9]. Thereby, the graphene was found to keep its zero band gap and to stack quasi randomly orientated on the h-BN substrate.

In this letter, we analyze the adhesion behavior and the electronic structure of graphene on h-BN from first-principles. We show that methods beyond standard density functional theory (DFT) are necessary to describe the weak non-local attraction between the h-BN and the graphene layers. We calculate adhesion energies using the random phase approximation (RPA) within the framework of the adiabatic connection fluctuation-dissipation theorem (ACFDT). On the basis of elasticity calculations, we discuss mechanisms to release the stress resulting from the lattice mismatch and leading to the formation of Moiré superstructures. By means of band structure calculations we obtain a low energy tight-binding description of graphene on h-BN and find mass terms which change their sign with the stacking configuration.

DFT is a successful approach to describe ground state properties of solids. However, widely used semilocal approximations for the exchange-correlation energy like the local density approximation (LDA) and generalized gradient approximation (GGA) [10] do not take long-range correlations into account correctly. Thus, they fail to reproduce van der Waals attraction and the prediction of equilibrium geometries of van der Waals bound layered systems, such as graphite or h-BN, proves problematic with these methods [11, 12]. A highly accurate means to describe van der Waals forces from first-principles is provided by the random phase approximation to the correlation energy [13]. Evaluated in the ACFDT framework, the RPA correlation energy reads [14]

$$E_c^{\text{RPA}} = \int_0^\infty \frac{d\omega}{2\pi} \text{Tr} \{ \ln[1 - \nu \chi^{\text{KS}}(i\omega)] + \nu \chi^{\text{KS}}(i\omega) \}, \quad (1)$$

where  $\chi^{\text{KS}}$  is the response function of the non-interacting Kohn-Sham (KS) system and  $\nu = \sum_{i<j} \frac{e^2}{|\vec{r}_i - \vec{r}_j|}$  the electron-electron interaction. Together with the total KS Hartree-Fock energy, usually referred to as exact exchange energy  $E_{\text{EXX}}$  [15], the total ground-state energy of the system reads as  $E = E_{\text{EXX}} + E_c^{\text{RPA}}$ . The ACFDT-RPA method has been proven accurate to describe bulk properties of solids such as lattice constants as well as adsorption energies [15]. For layered van der Waals bonded systems ACFDT-RPA yields a much more accurate description of the structural properties than LDA and vdW DFT methods [16, 17].

To simulate the graphene-h-BN system in this way, calculations were performed with the Vienna *ab initio* simulation package (VASP) [18] using plane wave basis sets within the projector-augmented wave (PAW) method [19]. To this end, a unit cell (4 atoms) containing graphene on an h-BN layer with  $25\text{\AA}$  of vacuum above was constructed. Six stacking configurations were considered (Fig. 1a): starting from configuration I, the graphene sheet was translated downwards by half a B-N

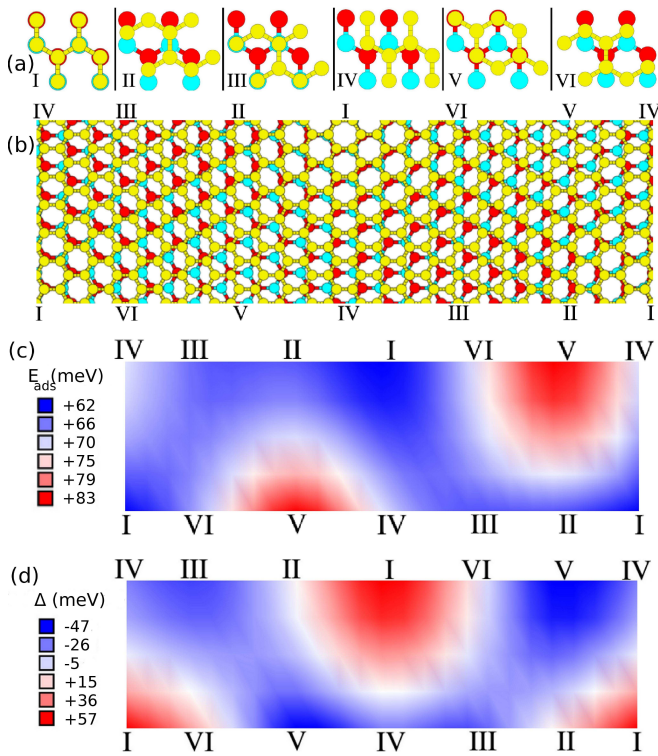


Figure 1. (Color online) (a) Top view of the calculated stacking configurations for graphene on h-BN with the carbon atoms (yellow), boron (red) and nitrogen (light blue). Between each neighboring images the graphene lattice is shifted downwards by half a B-N bond. (b) Moiré structure with persisting lattice mismatch. A lattice mismatch of 1.8% corresponds to a  $55 \times 55$  Moiré unit cell. For clarity, a smaller Moiré unit cell ( $13 \times 13$ ) is shown. (c) Adhesion energy ( $E_{\text{ads}}$ ) landscape in the Moiré pattern (color-coded). (d) The same for the local sublattice symmetry breaking  $\Delta$ .

bond length in each step until the initial configuration was reached again. The lattice constant was chosen to  $2.49 \text{ \AA}$ , referring to the LDA optimized lattice constant of h-BN (a discussion of the lattice mismatch follows below).  $\chi^{KS}$ ,  $E_c^{\text{RPA}}$  and  $E_{\text{EXX}}$  were evaluated with the LDA KS orbitals. In these computationally demanding simulations, convergence of the results was reached at a kinetic energy cut-off of 347 eV for the response function, a plane wave cut-off of 520 eV and a mesh of  $7 \times 7 \times 1$  k-points. Additionally, standard LDA/GGA calculations were performed for the same geometries with a  $24 \times 24 \times 1$  k-points grid and a kinetic energy cut-off of 500 eV.

Fig. 2 shows the RPA total energies per unit cell (relative to the energy at large separation) for the different stacking configurations as a function of the interlayer spacing  $d$ . The curves show that, starting from the highest-energy configuration I, the lowest-energy configuration V is approached step-wise. The configurations I, II and III exhibit total energy minima at interlayer spacings between  $3.50 \text{ \AA}$  and  $3.55 \text{ \AA}$ , whereat II and III are energetically virtually equivalent with minima of -

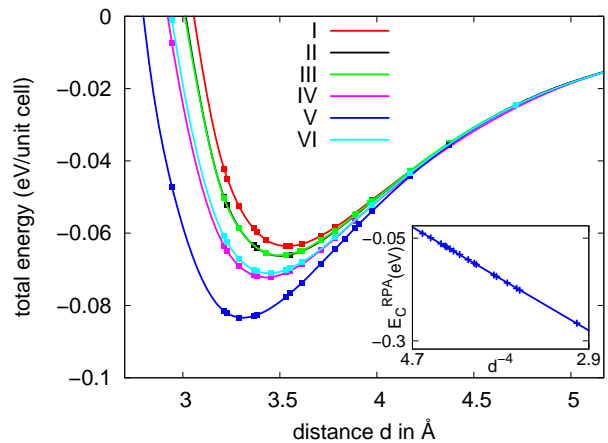


Figure 2. (Color online) Total RPA energies per unit cell for the stacking configurations I-VI as a function of the distance,  $d$ , between the graphene and h-BN layer. Inset: RPA correlation energy (relative to the correlation energy at large separation) of configuration V as function of  $d^{-4}$  between  $2.9 \text{ \AA}$  and  $4.7 \text{ \AA}$ .

65 meV; the minimum of configuration I is only slightly higher ( $-62 \text{ meV}$ ). Configuration V, where the carbon atoms sit on top of a boron atom and in the middle of the BN hexagon, is energetically most favorable with a minimum of  $-83 \text{ meV}$  and an equilibrium layer distance of  $3.35 \text{ \AA}$ . Energetically closest to V are IV ( $-71 \text{ meV}$ ) and VI ( $-70 \text{ meV}$ ), where the nitrogen atom is also not covered by a C atom or a C-C bond. The curves exhibit no additional energy barrier for translation. For distances larger than  $4 \text{ \AA}$ , all configurations become energetically indistinguishable.

To get further insight to the nature of the attractive forces between graphene and h-BN, we analyze the decay of the RPA correlation energy  $E_c^{\text{RPA}}$  with the interlayer spacing  $d$  (Fig. 2 inset). We find  $E_c^{\text{RPA}} \sim d^{-4}$ . This is clearly different from an exponential falloff as would be expected for local correlation effects as included in LDA or GGA. It rather indicates bonding of vdW type which yields power law decays  $E_c^{\text{RPA}} \sim d^{-p}$  [11] with  $p = 4$  for 2D insulating systems [11, 12].

A comparison of the RPA calculations with the standard LDA and GGA methods is given in Fig. 3. The LDA (see also [20]) yields a qualitatively correct equilibrium layer separation but underestimates the RPA adhesion energy by about 30%. The GGA, actually an improvement over the LDA in many cases [10], exhibits an even more dramatic underbinding with a weak minimum giving a negligible adhesion energy of less than 6 meV/unit cell at an extremely high equilibrium distance. The LDA and GGA curves nearly coincide for distances larger than  $4.5 \text{ \AA}$  and underestimate the van der Waals interaction also in this asymptotic region. The results clearly show that long-range correlations have to be taken

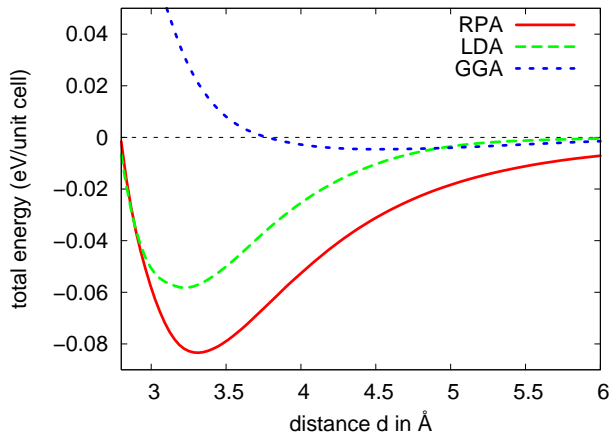


Figure 3. (Color online) Total energies per unit cell of configuration V from RPA, LDA and GGA.

into account for an accurate description of the layer attraction.

We now turn to the discussion of the elastic properties in order to judge the role of lattice mismatch effects. To this end, we determine the isotropic Young's modulus of single h-BN sheets from LDA and GGA calculations (the elastic properties of graphene have been widely investigated in experiment [21, 22] and theory [23]). These elastic constants are determined by strong in-plane chemical bonds and well described within the LDA/GGA [24]. For single h-BN sheets, the two-dimensional Young's modulus is defined by

$$Y_{2D} = \frac{1}{A_0} \left. \frac{\partial^2 E_s}{\partial \epsilon^2} \right|_{\epsilon=0}, \quad (2)$$

where  $\epsilon$  is the axial strain,  $E_s$  the total strain energy and  $A_0$  the equilibrium surface. The strain energies of a h-BN sheet were evaluated with uniaxial strains between -8% (compression) and 8% (tension). We obtain the two-dimensional Lamé parameters and Young's moduli of  $\lambda = 59\text{N/m}$ ,  $\mu = 125\text{N/m}$  and  $Y_{\text{h-BN},2D} = 309\text{N/m}$  within LDA and  $\lambda = 54\text{N/m}$ ,  $\mu = 123\text{N/m}$ ,  $Y_{\text{h-BN},2D} = 300\text{N/m}$  within GGA. The  $Y_{\text{h-BN},2D}$  correspond to three-dimensional Young's moduli of  $Y_{\text{h-BN},3D} = 0.94\text{TPa}$  (LDA) and  $Y_{\text{h-BN},3D} = 0.91\text{TPa}$  (GGA), assuming an interlayer separation of  $3.3\text{Å}$  [6]. Our full potential PAW calculations yield about 10% higher elastic constants  $Y_{\text{h-BN},2D}$  and  $\mu$  than calculations using Gaussian basis sets [25]. Our results are in agreement with the experiment, where  $Y_{\text{h-BN},2D,\text{exp}} \approx 220 - 510\text{N/m}$  was obtained for few-layer h-BN [26]. Compared to graphene, where  $Y_{G,2D} \approx 340\text{N/m}$  ( $Y_{G,3D} \approx 1.0\text{TPa}$ ) [21], the stiffness of h-BN is on the same order (about 10% smaller) and thus remarkably high.

With this background, we discuss the consequences of the lattice mismatch (1.8% in LDA and 1.9% in GGA) between the graphene and the h-BN and address the

question whether stacking disorder or Moiré superstructures should occur. To this end, we estimate the total energy difference of a structure with stacking according to the minimum energy configuration V in the entire sample and a Moiré structure with persisting mismatch (Fig. 1b). In the former case, the lattice mismatch must be overcome by strain forcing graphene and h-BN to have the same lattice constant to reach the lowest-energy configuration V in all regions of the sample. Due to the remarkable stiffness of both materials, buckling is suppressed and our calculations did not find any out-of-plane corrugations within the unit cell. This is in agreement with the experiments from Ref. [8]. In order to compensate the lattice mismatch, an isotropic compression of h-BN is energetically similarly favorable as a stretching of the graphene. Naturally, the energetically lowest configuration is a composition of stretched graphene and a compressed h-BN. We obtain an optimized lattice constant of  $2.467\text{Å}$  (LDA) with the total strain energy being  $18\text{meV/unit cell}$ , where anharmonic effects have been taken into account.

In the case of persisting mismatch in the system, a Moiré pattern with a large unit cell ( $55 \times 55$  for 1.8% mismatch) is formed (Fig. 1b). Here, out-of-plane corrugations resulting from interlayer spacings varying between  $3.35\text{Å}$  (region V) and  $3.55\text{Å}$  (region I) are negligible, since their amplitude ( $0.2\text{Å}$ ) is small as compared to their wavelength ( $\sim 135\text{Å}$ ). Hence, we focus on in-plane deformations. It is visible from Fig. 1b that our choice of stacking configurations I–VI simulated in RPA covers the sample uniformly and gives a sketch of the energy landscape (Fig. 1c). Those parts of the Moiré, where the nitrogen atoms are mainly beneath the center of the carbon rings (regions IV–VI), are energetically more favorable than regions I–III. For the Moiré structure we estimate the average adhesion energy per two carbon atoms by the average over the adhesion energies of the configurations I–VI. We obtain an average adhesion energy of  $69\text{meV}/(2\text{ C-atoms})$ . This is  $14\text{meV}/(2\text{ C-atoms})$  less than the adhesion energy of  $83\text{meV}/(2\text{ C-atoms})$  in configuration V. Therefore, total strain energy of  $18\text{meV}/(2\text{ C-atoms})$  overcompensates the adhesion energy gain when forcing the entire sample to configuration V. Hence, the lattice mismatch between the graphene and the h-BN will at least partly persist and strain will be released by realizing different stacking configurations as in the Moiré structure depicted in Fig. 1. This explains why multiple stacking configurations have been realized in the experiment of Ref. [8] and also explains the recent observations of Moiré patterns in STM experiments [27].

We now investigate the band structure modification in the Moiré structure. To this end, we calculated the band structure of all geometries depicted in Fig. 1a within the LDA. For configurations II, IV and VI we detect a small motion of the Dirac point in the hexagonal Brillouin zone away from the K to the M point (IV, VI)

	I	II	III	IV	V	VI
$\Delta(\text{meV})$	+57	+7	-34	-25	-47	+14
$1 - \tilde{t}/t$	0	0.010	0	-0.002	0	-0.010

Table I. Band gap  $\Delta$  with a positive sign corresponds to states close to valence band maximum being entirely localized in sublattice B, whereas  $\Delta < 0$  corresponds to states at valence band maximum being localized in sublattice A. The average band gap is -4 meV.  $\tilde{t}/t$  denotes the hopping  $\tilde{t}$  relative to  $t = 2.45\text{eV}$ .

and in the opposite direction (II). Mapping the problem on a nearest-neighbor tight-binding model, we see that a description of graphene in configurations II, IV and VI requires two different hopping parameters,  $t$  and  $\tilde{t}$ , as the threefold symmetry of the graphene nearest neighbor bonds is broken — analogous to the case of uniaxially strained graphene [3]. Fits of the TB model to the DFT results yield constant  $t = 2.45\text{eV}$  in all regions and  $\tilde{t} \neq t$  in regions II, IV and VI (Table I). In agreement with [20], we extract finite band gaps in all regions varying between 7 meV and 57 meV. However, we find that these gaps have different signs (Table I). In a Moiré structure like in Fig. 1d this leads to a landscape of local sublattice symmetry breaking  $\Delta$  with changing signs (Fig. 1d) and an average gap as small as -4 meV. Hence, we expect an absolute gap which is at least an order of magnitude smaller than the maximum local values of  $|\Delta|$ . This is well in line with the absence of a gap being reported in transport [8] and STM experiments [27].

In summary, we have calculated accurate adhesion energies for graphene-h-BN systems by means of RPA simulations in the framework of the ACFDT. A comparison to LDA/GGA calculations showed that the description of the weak binding of graphene on h-BN through van der Waals forces requires methods beyond standard semilocal density functionals. A comparison of the strain energies with the adhesion energy differences suggest that a lattice mismatch between will persist. This explains the experimental observation of different stackings, Moiré patterns, and stacking disorder. Interestingly, the strain energy to force graphene and hBN at the same lattice constant (18 meV/2C atoms) and the adhesion energy cost to realize the Moiré pattern of Fig. 1b (14 meV/2C atoms) are quite close. Therefore, graphene-hBN hybrid structures are likely very sensitive to external strain. It remains to be seen to which extent these systems are suitable as strain sensors or for strain engineering of their electronic properties.

Support from the DFG (Germany) via SFB 668 and Priority Programme 1459 "Graphene", FOM (The

Netherlands), and computer time at HLRN (Germany) are acknowledged. We thank G. Kresse for helpful discussions.

\* bsachs@physnet.uni-hamburg.de

† twehling@physnet.uni-hamburg.de

- [1] M. Ishigami *et al.*, Nano Lett. **7**, 1643 (2007).
- [2] V. Geringer *et al.*, Phys. Rev. Lett. **102**, 76102 (2009).
- [3] M. I. Katsnelson and A. K. Geim, Phil. Trans. R. Soc. A **366**, 195 (2008); T. O. Wehling *et al.*, EPL **84**, 17003 (2008).
- [4] K. Nomura and A. H. MacDonald, Phys. Rev. Lett. **96**, 256602 (2006); T. Ando, J. Phys. Soc. Jpn. **75**, 074716 (2006); E. H. Hwang, S. Adam, and S. Das Sarma, Phys. Rev. Lett. **98**, 186806 (2007); S. Adam *et al.*, Proc. Natl. Acad. Sci. **104**, 18392 (2007); C. Jang *et al.*, Phys. Rev. Lett. **101**, 146805 (2008).
- [5] Y.-J. Kang, J. Kang, and K. J. Chang, Phys. Rev. B **78**, 115404 (2008); S. Sonde *et al.*, Appl. Phys. Lett. **97**, 132101 (2010).
- [6] W. Paszkowicz *et al.*, Appl. Phys. A: Mat. Sci. & Proc. **75**, 431 (2002).
- [7] K. Watanabe, T. Taniguchi, and H. Kanda, Nature Materials **3**, 404 (2004).
- [8] C. R. Dean *et al.*, Nature Nanotechnology **5**, 722 (2010).
- [9] I. Meric *et al.*, Arxiv preprint arXiv:1101.4712 (2011).
- [10] J. P. Perdew, K. Burke, and Y. Wang, Phys. Rev. B **54**, 16533 (1996); J. P. Perdew, K. Burke, and M. Ernzerhof, Phys. Rev. Lett. **77**, 3865 (1996).
- [11] J. F. Dobson, A. White, and A. Rubio, Phys. Rev. Lett. **96**, 73201 (2006).
- [12] H. Rydberg *et al.*, Phys. Rev. Lett. **91**, 126402 (2003).
- [13] J. P. Perdew and Y. Wang, Phys. Rev. B **45**, 13244 (1992); D. C. Langreth and J. P. Perdew, *ibid.* **15**, 2884 (1977).
- [14] Y. M. Niquet, M. Fuchs, and X. Gonze, Phys. Rev. A **68**, 032507 (2003).
- [15] J. Harl, L. Schimka, and G. Kresse, Phys. Rev. B **81**, 115126 (2010).
- [16] J. Harl and G. Kresse, Phys. Rev. Lett. **103**, 56401 (2009).
- [17] A. Marini, P. García-González, and A. Rubio, Phys. Rev. Lett. **96**, 136404 (2006).
- [18] G. Kresse and J. Hafner, J. Phys. Cond. Matter **6**, 8245 (1994).
- [19] P. E. Blöchl, Phys. Rev. B **50**, 17953 (1994); G. Kresse and D. Joubert, *ibid.* **59**, 1758 (1999).
- [20] G. Giovannetti *et al.*, Phys. Rev. B **76**, 073103 (2007).
- [21] C. Lee *et al.*, Science **321**, 385 (2008).
- [22] C. Gómez-Navarro, M. Burghard, and K. Kern, Nano Lett. **8**, 2045 (2008).
- [23] S. Bera *et al.*, Phys. Rev. B **82**, 195445 (2010).
- [24] F. Liu, P. Ming, and J. Li, Phys. Rev. B **76**, 064120 (2007).
- [25] K. N. Kudin, G. E. Scuseria, and B. I. Yakobson, Phys. Rev. B **64**, 235406 (2001).
- [26] L. Song *et al.*, Nano Lett. **10**, 3209 (2010).
- [27] J. Xue *et al.*, Nature Materials **10**, 282 (2011).